Hybrid Reconfigurable Battery Pack for All-Electric Aircraft
Synergizing High-Specific-Energy and Power Battery Types

Bhide, Mayuresh; Liang, Yawen; Mouli, Gautham Ram Chandra; Ghaffarian Niasar, Mohamad; Bauer, Pavol

Citation (APA)
Bhide, M., Liang, Y., Mouli, G. R. C., Ghaffarian Niasar, M., & Bauer, P. (2024). Hybrid Reconfigurable Battery Pack for All-Electric Aircraft: Synergizing High-Specific-Energy and Power Battery Types. In *Proceedings of the 2024 IEEE Transportation Electrification Conference and Expo (ITEC)* IEEE. https://doi.org/10.1109/ITEC60657.2024.10598954

Important note
To cite this publication, please use the final published version (if applicable).
Please check the document version above.

Hybrid Reconfigurable Battery Pack for All-Electric Aircraft: Synergizing High-Specific-Energy and Power Battery Types

Mayuresh Bhide, Yawen Liang, Gautham Ram Chandra Mouli, Mohamad Ghaffarian Niasar and Pavol Bauer
Deptartment of Electrical Sustainable Energy
Delft University of Technology
Delft, Netherlands

Abstract—The aviation industry, responsible for over 2% of energy-related CO_2 emissions in 2022, aims for Net Zero Emissions by 2050. Despite electric aircraft's environmental benefits and improved operational efficiency, the current battery technology limits their range and size. Based on the optimal system voltage and power profile of the reference all-electric aircraft, this paper presents the design of a hybrid reconfigurable battery pack. The design incorporates a combination of high-specific-energy ($263\,\mathrm{W\,h\,kg^{-1}}$ at cell level) and high-specific-power ($1800\,\mathrm{W\,kg^{-1}}$ at cell level) battery types and its performance is compared with that of a fixed configuration battery pack comprising a single battery type. Simulation results suggest a potential $900\,\mathrm{kg}$ (18% lighter than fixed configuration) weight savings with reconfigurable pack, translating into enhanced payload, energy savings, or range extension for 9 PAX Eviation Alice electric aircraft at just 0.4% more energy capacity loss in 500 cycles.

I. INTRODUCTION

Globally, commercial air operations account for approximately 2% of the energy-related CO_2 emissions [1], [2]. A shift towards electric aircraft is inevitable to mitigate CO_2 emissions and to reduce dependence on jet fuel. All-electric aircraft emerges as a promising solution for sustainable future aviation, offering the potential for zero in-flight emissions, increased propulsion efficiency, greater scalability, redundancy, noise reduction, and lower operational costs [3], [4], [5]. However, aircraft electrification is presently limited by the existing battery technology mainly due to its low specific energy and power [6]. Several papers have explored the concept of reconfigurability in battery packs, as highlighted in [7], [8]. This approach allows cell configuration adjustment based on specific load demands, utilizing reconfigurability for fault tolerance and dynamic cell balancing. However, the application of reconfigurable battery packs for electric aircraft remains relatively unexplored. In addition to the advantages highlighted in prior research, reconfigurability can facilitate the simultaneous operation of a hybrid battery pack comprising different cell types. This is particularly beneficial for all-electric aircraft, where the battery pack needs to feature both high specific power for takeoff and climbing, as well as high specific energy for cruising. By leveraging the strengths of each cell type according to the specific phases of aircraft operation, this study proposes a reconfigurable battery pack design using state-of-the-art Li-ion battery technology, aiming to optimize battery pack weight by implementing a hybrid battery pack configuration for all-electric aircraft.

A. Paper structure

This paper is structured as follows. The power profile during the flight mission and the system level voltage of the reference aircraft are discussed in section II. Section III covers the detailed design of the fixed and hybrid reconfigurable battery packs. The proposed battery pack configurations are thoroughly analyzed and compared in IV. Finally, section V concludes this article.

II. POWER PROFILE AND SYSTEM LEVEL VOLTAGE

A. Power profile

The design of a battery pack for an all-electric aircraft is tailored according to its power profile. The power profile encompasses eleven distinct phases, delineated into taxi-out, take-off, initial climb, final climb, cruise, descent, and landing phases during regular missions, and climb, cruise, landing, and taxi-in phases during reserve missions. To establish a power profile, reference electric aircraft, and their specifications are essential. In this paper, Eviation Alice is chosen as the reference aircraft. Table I presents the specifications of Eviation Alice according to [9], [10]. Based on the above specification, design-related assumptions according to each phase (e.g., coefficient of lift and drag, time duration, etc.), and performance indices (e.g., cruising speed, rate of climb, cruising altitude, takeoff distance, etc.), the power profile for each phase of the flight trip is calculated based on the mechanics of the aircraft [11], [12].

TABLE I
EVIATION ALICE SPECIFICATIONS [9], [10]

Specifications	Values
Max operating speed	260 ktas = $481.52\,\mathrm{km\,h^{-1}}$
Day VFR range	250 nm = 463 km
Maximum Take-Off Weight (MTOW)	18,400 lbs = $8346.1\,\mathrm{kg}$
Useful payload (commuter)	2,500 lbs = $1134\,\mathrm{kg}$
Power output	2x motors, $700\,\mathrm{kW}$ each
Maximum L/D ratio	18.5
Velocity to achieve maximum range	152 knots = $281.5\,\mathrm{km\,h^{-1}}$

Battery power profile
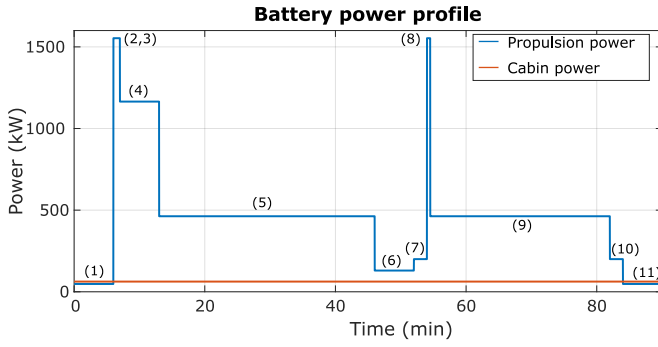
Fig. 1. Power profile for a single flight trip with a reserved mission of the Eviation Alice

Phase numbers	Phases	Battery power
(1), (11)	Taxi-out, Taxi-in	48 kW
(2), (3), (8)	Take-off, Initial climb, Reserve climb	1553 kW
(4)	Final climb	1165 kW
(5), (9)	Cruise, Reserve cruise	462 kW
(6)	Descent	130 kW
(7), (10)	Landing, Reserve landing	200 kW

Fig. 1 shows the power profile of a single flight trip with a reserved mission. The blue line denotes the battery power for propulsion, while the orange line represents the battery power necessary for cabin operation. Note that this power profile is plotted by taking into account 93% electric motor efficiency, 98% power electronics efficiency, and power cable losses occurring in the powertrain [10]. Table II shows the battery power corresponding to each phase. The peak propulsion power requirement (P_{max}) is the power demanded in the take-off and initial climb phase, where P_{max} = 1553.2 kW. The total propulsion energy requirement (E_{total}) from the battery system for regular and reserve mission phases is 657.3 kW h. Additionally, auxiliary power demands are factored in as cabin power. In this study, a constant cabin power of 60 kW is assumed throughout the entire flight mission while the total battery energy is 96 kW h for cabin operation [13].

B. System level voltage calculation

The selection of the system-level voltage for electric aircraft requires careful consideration as it influences the weight of the cables, battery terminal voltage, and related safety measures. A lower system voltage results in higher current magnitude and increased losses or increased conductor radius, while a higher system voltage may lead to the initiation of partial discharges and consequent insulation system failure. Therefore, optimizing the system-level voltage is necessary to minimize the cabling system's overall weight.

The power cable consists of multiple layers, including the power conductor, inner semiconductor, insulation, outer semiconductor, conducting shield, and outer jacket layers [14]. To achieve a cable with reduced weight, it's essential to ascertain the insulation thickness (t_i) and conductor radius (r_c). This study approximates the thicknesses of the inner and outer semiconducting layers ($t_{\text{isc}} = t_{\text{osc}} = 0.6$ mm), conducting shield ($t_s = 1$ mm), and the outer jacket ($t_{\text{oj}} = 1$ mm) together to be 3.2 mm, since these layers typically have a standard range of thickness values irrespective of the other design parameters [15], [16].

The objective function of optimization is given by (1), where the mass of the conductor (M_c) and insulator (M_i) are given by (2) and (3), M_x is a constant which denotes the summation of the masses of other layers whose thicknesses are constant, l is the cable length, ρ_c is the density of conducting material (aluminum), ρ_i is the density of insulation material (cross-linked polyethylene).

$$Min. \ M_{\text{cable}} = M_c + M_i + M_x \tag{1}$$

$$M_c = \rho_c \, l \, \pi \, r_c^2 \tag{2}$$

$$M_i = \rho_i \, l \, \pi \left((r_c + t_{\text{isc}} + t_i)^2 - (r_c + t_{\text{isc}})^2 \right) \tag{3}$$

The desired operating conductor temperature influences the size of the conductor radius. The conductor is assumed to operate at a temperature of 90°C or lower, and the conductor radius is calculated for the worst-case scenario with conductor temperature T_c = 90°C. The worst case scenario for ambient temperature T_{amb} = 40°C. The heat transfers within the cable and from the cable surface to the ambient are assumed to be conductive and convective respectively. Under steady-state conditions, the heat generated in the conductor is equal to the heat loss due to convection at the surface of the cable.

$$T_c - T_s = \frac{I^2}{\sigma \, \pi \, r_c^2} \frac{1}{2 \, \pi \, k} \left[\ln \left(1 + \frac{t_{\text{isc}} + t_i + t_{\text{osc}}}{r_c} \right) \right.$$
$$\left. + \ln \left(1 + \frac{t_{\text{oj}}}{r_c + t_i + t_{\text{isc}} + t_{\text{osc}} + t_s} \right) \right] \tag{4}$$

$$T_s - T_{\text{amb}} = \frac{I^2}{\sigma \, \pi \, r_c^2} \frac{1}{2 \, \pi \, r_c \, h} \tag{5}$$

$$t_i = r_c \left\{ exp \left[\frac{\left(\frac{3\epsilon}{1+2\epsilon} \right) V \, d_v}{\alpha \, r_c} \right] - 1 \right\} + C \tag{6}$$

The difference in conductor temperature and the surface temperature (T_s) is given by (4) where σ is the conductivity of the conductor, I is the conductor current, k is the thermal conductivity of the insulation. The difference in surface temperature and the ambient temperature (T_{amb}) is given by (5) where h is the convection thermal coefficient. The Single Void Discharge (SVD) method used in [17] is employed for calculating the thickness of the insulation layer t_i given in (6) where ϵ is the dielectric permittivity of the insulating material, V is the system level voltage, d_v is the thickness of void or inclusion and lastly α denotes the breakdown voltage of the air at flying

altitude. The constant C takes a value of $0\,\text{cm}$ for cables with voltages equal to or exceeding $20\,\text{kV}$ and $0.1\,\text{cm}$ for cables with lower voltages [15].

With two unknowns T_s and r_c, (4) and (5) are solved simultaneously after substituting (6) in (4). Based on (1), (2), and (3) the cable weight is calculated over a range of voltages to determine the voltage at which the weight of the cable is minimum. Fig. 2a shows that as the system voltage increases
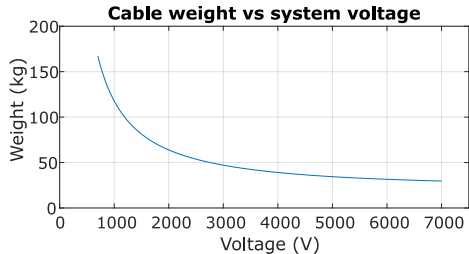
(a) Weight of the power cable over the range of system voltages
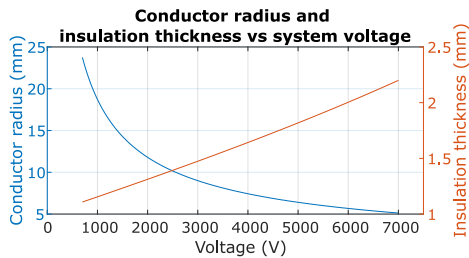
(b) Conductor radius and insulation thickness over the range of system voltages

Fig. 2. Change in parameters of power cables over the range of system voltages

the weight of the power cable reduces. The insulation thickness increase is much less than the reduction in the conductor radius as seen in Fig. 2b. Hence the characteristic of the cable weight curve closely resembles that of the conductor radius curve. In Fig. 2a, till the mark of $3\,\text{kV}$ the power cable weight reduction is drastic, and after that point, it reduces by a very small quantity while at higher voltages the risk of partial discharge at the low-pressure environment of the aircraft becomes severe for both the cabling system and motor winding insulation. Hence, considering this trade-off system level voltage of $3\,\text{kV}$ is selected. This voltage level falls within the range of voltages projected by the researchers for the anticipated system-level voltages of upcoming fully and hybrid electric aircraft [18], [5]. When designing the battery pack, it's essential to align the pack voltage with the system voltage. This alignment eliminates the necessity for a DC-DC converter. Additionally, voltage stabilization, ensuring a constant voltage output to the electrical bus, can be efficiently managed using a battery control unit [19].
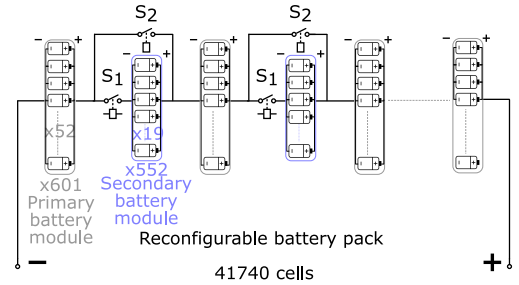
III. BATTERY PACK DESIGN

A. Fixed configuration battery pack

Li-NMC is recognized as a suitable battery chemistry for small electric aircraft, attributed to its high specific energy
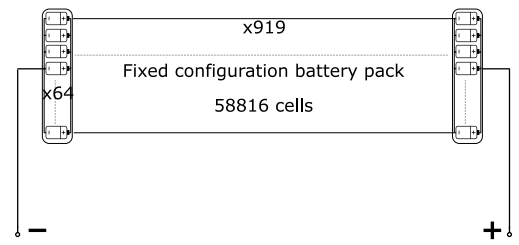
(a) Fixed configuration battery pack

(b) Reconfigurable battery pack

Fig. 3. Schematic of both battery packs

[6], which is a critical performance metric that determines the flight range and payload capacity, while specific power determines take-off and climb performance. Hence, a high-specific energy cell (LG-INR21700-M50) and a high-specific power cell (SAMSUNG-INR21700-40T) are shortlisted to form two fixed-configuration battery packs where each battery pack exclusively employs a single type of battery cell. Table III shows the cell and pack level specifications and their weight with 82% packing efficiency as per [20] to fulfill the energy and power requirement of the reference electric aircraft. Note that the battery packs are sized to power both propulsive and cabin loads. Due to the low C-rate of the LG-M50 cell, extra cells (~ 1.43 times) are required to satisfy the power demand compared to the energy demand. On the other hand, due to the low specific energy of the SAMSUNG-40T cell, more than double cells are required to satisfy the energy demand compared to the power demand. Since the LG-M50 battery pack's weight is less than that of the SAMSUNG-40T battery pack, the LG-M50 battery pack has been chosen as the fixed configuration battery pack.

For the module, there are two types of cell configurations for the electrical connections: series cell module (SCM) and parallel cell module (PCM). In SCM, cells are connected in series to make up a module, and such modules are connected in parallel to make up a pack. In PCM, cells are connected in parallel to make up a module, and such modules are connected in series to make up a pack. [21], [22] stated that the PCM structure can realize capacity maximization and is more suitable for high-power applications. Moreover, PCM offers a self-balancing feature at the cell level, which is crucial in large-scale battery packs since a dedicated balancing circuit inside each module is a complex procedure. Hence, the PCM structure is employed for the proposed fixed and reconfigurable

battery packs. Therefore, the total cell number of the fixed configuration battery pack is 58816 which requires 919 PCM modules in series and 64 cells in each PCM, as shown in Fig. 3a.

TABLE III
CELL AND PACK SPECIFICATIONS

		LG-M50	SAMSUNG-40T
Cell	Sp. energy	$263\,\mathrm{W\,h\,kg^{-1}}$	$205\,\mathrm{W\,h\,kg^{-1}}$
	Sp. power	$382\,\mathrm{W\,kg^{-1}}$	$1028\,\mathrm{W\,kg^{-1}}$
	Nom. energy	18.2 W h	14.4 W h
	Nom. voltage	3.63 V	3.6 V
	Peak discharge C rate	1.5	5
Pack	Number of cells	58816	59960
	Weight	4950 kg	5120 kg

B. Hybrid reconfigurable battery pack

To capitalize on the strengths of high-specific-energy and high-specific-power battery types, a hybrid reconfigurable battery pack design is proposed to fulfill propulsive power and energy needs throughout a flight. In this design, the high-specific-energy LG-M50 battery modules called the 'primary battery modules,' are complemented with the high-specific-power SAMSUNG-40T battery modules, called the 'secondary battery modules' during phases of high power demand. The objective of the primary battery modules is to fulfill the energy demand, and the secondary modules are intended to meet the power demand during moments of peak power namely take-off, initial climb, final climb, and reserve climb phases, as shown in Fig. 1. Besides, a dedicated LG-M50 battery pack for powering cabin loads is assumed. Note that the weight of this battery pack is considered while comparing the total battery pack weight of fixed and reconfigurable battery packs.

The cell configuration optimization is carried out using the *fmincon* solver in MATLAB. The following are the equations of the cell configuration optimization ($N = [N_{1P}, N_{1S}, N_{2P}, N_{2S}]$) in the hybrid reconfigurable battery pack where N_{1P}: cells in parallel within the primary battery module, N_{1S}: primary battery modules in series, N_{2P}: cells in parallel within the secondary battery module, N_{2S}: secondary battery modules in series. The objective function for the reconfigurable battery pack is to minimize the battery pack weight W_{pack}, as illustrated in (7). Three nonlinear constraints from (8) to (10) express energy and power requirements during the flight mission.

$$Min.\ W_{\mathrm{pack}} = N_{1\mathrm{P}}\,N_{1\mathrm{S}}\,W_{\mathrm{c,LG}} + N_{2\mathrm{P}}\,N_{2\mathrm{S}}\,W_{\mathrm{c,Samsung}} \quad (7)$$

Non-linear constraints:

$$I_{\mathrm{c,LG}}\,N_{1\mathrm{P}}\,(N_{1\mathrm{S}}\,V_{\mathrm{c,LG}} + N_{2\mathrm{S}}\,V_{\mathrm{c,Samsung}}) > P_{\mathrm{max}} \quad (8)$$

$$I_{\mathrm{c,Samsung}}\,N_{2\mathrm{P}}\,(N_{1\mathrm{S}}\,V_{\mathrm{c,LG}} + N_{2\mathrm{S}}\,V_{\mathrm{c,Samsung}}) > P_{\mathrm{max}} \quad (9)$$

$$N_{1\mathrm{P}}\,N_{1\mathrm{S}}\,E_{\mathrm{c,LG}} + N_{2\mathrm{P}}\,N_{2\mathrm{S}}\,E_{\mathrm{c,Samsung}} > E_{\mathrm{total}} \quad (10)$$

where, W_c, I_c, V_c, and E_c are weight, max discharge current, nominal voltage, and energy at the cell level, respectively.

The primary and secondary battery modules are connected in series. If connected in parallel, the net battery pack current will get divided into parallel branches, negating the intention of using high-discharge C-rate secondary battery modules. Further, the lower bounds of N_{1S} are assigned to identify the local minimum that ensures the battery pack voltage is close to the system-level voltage in II-B. During the optimization process, the module current remains consistent across all modules as they are interconnected in series.

The optimization yields $N = [52, 601, 19, 552]$, as shown in Fig 3b. There are 52 cells in parallel for each primary battery module, while for the secondary battery module, there are 19 cells in parallel. There are 601 primary and 552 secondary battery modules in series for the reconfigurable battery pack. For reconfigurability, the LG (primary) module and the SAMSUNG (secondary) module can be connected in series through a power switch S_1, and the SAMSUNG module can be bypassed using the power switch S_2. The switches used are assumed to have a small resistance of $1\,\mathrm{m\Omega}$. This optimized hybrid reconfigurable battery pack results in voltages of $2181.63\,\mathrm{V}$ (when the primary modules are operational individually) and $4168.83\,\mathrm{V}$ (when both battery modules are connected in series). These voltages are comparatively closer to the optimum system-level voltage than the other optimization results. Hence, this configuration is chosen as the design for the hybrid reconfigurable battery pack. Table IV summarized the specifications of fixed and hybrid reconfigurable battery packs.

TABLE IV
SPECIFICATIONS OF FIXED AND HYBRID RECONFIGURABLE BATTERY PACKS

|	Fixed configuration	Hybrid reconfigurable
Rated power	$1553.25\,\mathrm{kW}$	$1580.44\,\mathrm{kW}$
Rated energy	$1067.5\,\mathrm{kW\,h}$	Primary modules: $567.2\,\mathrm{kW\,h}$ Secondary modules: $151\,\mathrm{kW\,h}$ Total: $718.2\,\mathrm{kW\,h}$
Number of cells	58816	Primary cells: 31252 Secondary cells: 10488 Total: 41740
Weight	$4950\,\mathrm{kg}$	Primary modules: $2629.7\,\mathrm{kg}$ Secondary modules: $895.3\,\mathrm{kg}$ Cabin load battery: $512\,\mathrm{kg}$ Total: $4037\,\mathrm{kg}$

IV. RESULT

A. Simulation validation

To simulate the performance of the fixed and hybrid reconfigurable battery pack, the battery packs were modeled using MATLAB/Simulink. Simulating a 90-minute flight trip involving thousands of cells demands high processing power and duration. Hence, the aircraft power profile is normalized to a pair of primary and secondary modules. The control logic of the reconfigurable hybrid battery pack is shown in (11).
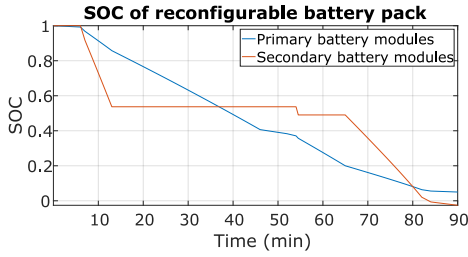
(a) SOC of the hybrid reconfigurable battery pack
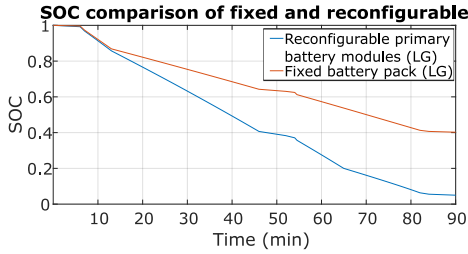
(b) SOC of both configurations.

Fig. 4. SOC change during a flight.

$$[S_1, S_2] = \begin{cases} [1,0], & \text{if } P_{\text{demand}} > P_{\text{max}}^{\text{primary}} \ || \ SOC_{\text{primary}} < 20\% \\ [0,1], & \text{otherwise} \end{cases}$$

(11)

If the power demand is lower than the power capability of primary battery modules ($P_{\text{max}}^{\text{primary}}$), the signal 'S$_1$' is given the command '0' or 'false', and the signal 'S$_2$' is given the command '1' or 'true'. Only the primary battery modules are in operation and the secondary battery modules are bypassed. If the power demand exceeds the power capability of primary battery modules ($P_{\text{max}}^{\text{primary}}$), the signal 'S$_1$' is given the command '1' or 'true', and the signal 'S$_2$' is given the command '0' or 'false'. Due to the high power demand, this switch status is employed in phases such as take-off, initial, final, and reserve climb, as shown in Fig. 1. Fig. 4a and Fig. 4b show the variation in SOC of the battery pack throughout the flight trip. During the reconfigurable battery pack sizing process, the energy constraint was met by mathematically summing up the nominal energy values of both the primary and secondary battery modules. However, since the primary battery modules operate for most of the trip duration, there is a potential scenario where the primary modules may deplete to zero state-of-charge (SOC) during the reserved mission phase, leaving all the remaining energy in the secondary battery modules. To mitigate this, the SOC value of the primary battery modules is provided to the control logic function. If the SOC value of primary battery modules falls below 20%, the secondary battery modules will be connected in series, thus averting the complete depletion of the primary battery modules. The reflection of this event can be seen in Fig. 4a where at the 65 min mark, the SOC of the primary modules touches the value of 0.2, and as it depletes further, the secondary modules are connected in series, and its SOC starts to drop.

B. Weight saving

After a complete flight mission, Fig. 4b illustrates that the fixed configuration LG-M50 battery pack retains more than half of the battery capacity after a flight mission. The remaining energy in the fixed configuration battery pack underscores that the sizing of the fixed configuration battery pack is primarily influenced by the high power demand during take-off and climbing phases due to the low specific power of the LG-M50 cell.

For the hybrid reconfigurable battery pack, the primary battery modules utilize 92% of the battery capacity during a flight mission. A total weight of which is $4037 \, \text{kg}$. Assuming the weight of power switches per module to be relatively negligible, the weight difference between the reconfigurable battery pack and the fixed configuration battery is near $900 \, \text{kg}$ (18% lighter than the fixed configuration battery pack).

C. Cell aging

Since there are more cells in the fixed configuration battery pack, intuitively, the aging of the battery pack should be less than the reconfigurable battery pack. Thus to quantify this characteristic, the cell aging performance was estimated using PyBaMM. PyBaMM contains various battery parameter sets, and the LG-M50 cell parameter set is used. It is based on the experimental studies by [23], [24] and the results are generated using the Doyle Fuller Newman model. While scripting the aging algorithm in PyBaMM, it is assumed that the temperature is kept constant at 25°C using an onboard thermal management system. 500 cycles with a discharging current profile from the Simulink battery model and the CC-CV (0.3 C-rate, 4.2V) charging profile recommended in the cell datasheet are executed. The aging performance modeling focuses on the loss of lithium inventory (LLI) caused by SEI growth, lithium plating, and side reactions, indicating the depletion of active lithium ions available for cycling [25].

As illustrated in Fig. 5a, the cell current from the primary battery modules of the hybrid reconfigurable configuration is higher than the fixed configuration. Fig. 5b shows that the capacity loss due to the previously mentioned causes of LLI is greater in the primary battery modules of the reconfigurable battery pack compared to the fixed-configuration battery pack due to the comparatively high discharge C-rate during the flight mission. However, the difference in the capacity loss of these configurations is almost $0.02 \, \text{A h}$ after 500 cycles, meaning the LG-M50 cell in the reconfigurable battery pack holds only 0.4% more capacity losses than the LG-M50 cell in the fixed configuration battery pack. It should be noted that the LLI aging model is a simplified representation of the complex degradation process occurring inside the cell and hence limits the accuracy of the results due to ignoring factors such as mechanistic details, temperature effects, electrolyte dynamics, etc.

V. CONCLUSION

The electric aircraft battery pack sizing is determined both by energy and power requirements. The proposed hybrid
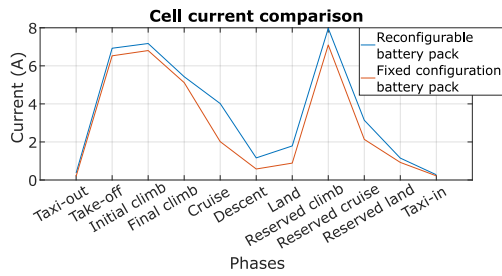
(a) Cell current of both configurations.
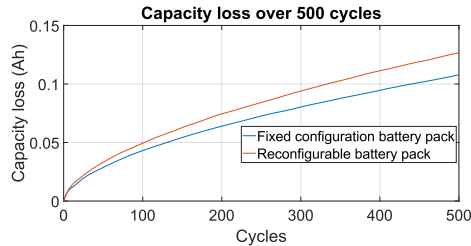
(b) Capacity loss for both configurations.

Fig. 5. Aging performance of fixed and hybrid reconfigurable battery pack after 500 cycles.

reconfigurable battery pack leverages the strengths of each cell type in terms of its high specific energy and high specific power, which connects the secondary battery modules in series when the propulsion power demand exceeds the primary modules' nominal power. Using the Eviation Alice aircraft and the LG-M50 and SAMSUNG-40T cells as a reference, a reduction of 900 kg in battery weight (18% reduction in weight) can be achieved compared to the fixed configuration battery pack at the cost of 0.4% more capacity loss after 500 cycles. The weight savings can translate into enhanced cargo capacity, energy savings, and range extension. While we have demonstrated a hybrid battery pack using a particular high-specific energy cell (LG-INR21700-M50) and a high-specific power cell (SAMSUNG-INR21700-40T), the concept can be extended to any combination cells that complement each other in terms of high-specific energy and high-specific power.

The dynamics of the system during battery reconfiguration, the hardware design of the switches and their control, the power converter architecture, and the safety considerations for the battery pack are beyond the current scope and will be addressed in future research.

REFERENCES

[1] G. M. Bravo, N. Praliyev, and Árpád Veress, "Performance analysis of hybrid electric and distributed propulsion system applied on a light aircraft," *Energy*, vol. 214, p. 118823, 2021.

[2] IEA, "Tracking clean energy progress 2023 – analysis," Jul 2023. [Online]. Available: https://www.iea.org/reports/tracking-clean-energy-progress-2023

[3] A. R. Gnadt, R. L. Speth, J. S. Sabnis, and S. R. Barrett, "Technical and environmental assessment of all-electric 180-passenger commercial aircraft," pp. 1–30, 2 2019.

[4] A. Schwab, A. Thomas, J. Bennett, E. Robertson, and S. Cary, "Electrification of Aircraft: Challenges, Barriers, and Potential Impacts," National Renewable Energy Lab.(NREL), Golden, CO (United States), Tech. Rep., 2018. [Online]. Available: https://www.nrel.gov/docs/fy22osti/80220.pdf.

[5] S. Sahoo, X. Zhao, and K. Kyprianidis, "A review of concepts, benefits, and challenges for future electrical propulsion-based aircraft," *Aerospace*, vol. 7, no. 4, 4 2020.

[6] Y. Liang, G. R. C. Mouli, and P. Bauer, "Charging technology for electric aircraft: State of the art, trends, and challenges," *IEEE Transactions on Transportation Electrification*, 2023.

[7] T. Kim, W. Qiao, and L. Qu, "Power electronics-enabled self-X multicell batteries: A design toward smart batteries," *IEEE Transactions on Power Electronics*, vol. 27, no. 11, pp. 4723–4733, 2012.

[8] H. Kim and K. G. Shin, "DESA: Dependable, efficient, scalable architecture for management of large-scale batteries," *IEEE Transactions on Industrial Informatics*, vol. 8, no. 2, pp. 406–417, 5 2012.

[9] "Aircraft – Eviation." [Online]. Available: https://www.eviation.com/aircraft/

[10] F. Russo, "Eviation Alice analysis of aircraft performances and comparison with official claims," Tech. Rep., 2022.

[11] C. E. Riboldi, "An optimal approach to the preliminary design of small hybrid-electric aircraft," *Aerospace Science and Technology*, vol. 81, pp. 14–31, 2018.

[12] D. Raymer, *Aircraft design: a conceptual approach*. American Institute of Aeronautics and Astronautics, Inc., 2012.

[13] R. de Graaff and N. Fontenai, "Design of propulsion system for 9 pax electric aircraft: Motors and power distribution for aea," 2022.

[14] A. Shekhar, X. Feng, A. Gattozzi, R. Hebner, D. Wardell, S. Strank, A. Rodrigo-Mor, L. Ramírez-Elizondo, and P. Bauer, "Impact of DC Voltage Enhancement on Partial Discharges in Medium Voltage Cables-An Empirical Study with Defects at Semicon-Dielectric Interface," *Energies*, vol. 10, no. 12, p. 1968, 2017. [Online]. Available: www.mdpi.com/journal/energies

[15] E. Aretskin-Hariton, M. Bell, S. Schnulo, and J. S. Gray, "Power cable mass estimation for electric aircraft propulsion," in *AIAA AVIATION 2021 FORUM*, 2021, p. 3021.

[16] R. Paludo, G. C. da Silva, and V. S. Filho, "The study of semiconductor layer effect on underground cables with time domain reflectometry (tdr)," *IOSR Journal of Electrical and Electronics Engineering*, vol. 7, no. 6, pp. 1–7, 2013.

[17] F. C. Cheng, "Insulation Thickness Determination Of Polymeric Power Cables," *IEEE Transactions on Dielectrics and Electrical Insulation*, vol. 1, no. 4, pp. 624–629, 1994.

[18] R. Jansen, C. Bowman, and A. Jankovsky, "Sizing power components of an electrically driven tail cone thruster and a range extender," in *16th AIAA Aviation Technology, Integration, and Operations Conference*, 2016, p. 3766.

[19] A. Seitz, C. Pornet, A. T. Isikveren, P. C. Vratny, K. O. Plötner, and M. Hornung, "Conceptual Studies of Universally-Electric Systems Architectures Suitable for Transport Aircraft," DeutscherLuft und RaumfahrtKongress, DLRK, Berlin, Tech. Rep., 2012. [Online]. Available: https://www.researchgate.net/publication/274705769

[20] H. Löbberding, S. Wessel, C. Offermanns, M. Kehrer, J. Rother, H. Heimes, and A. Kampker, "From Cell to Battery System in BEVs: Analysis of System Packing Efficiency and Cell Types," *World Electric Vehicle Journal 2020, Vol. 11, Page 77*, vol. 11, no. 4, p. 77, 12 2020. [Online]. Available: https://www.mdpi.com/2032-6653/11/4/77/htm https://www.mdpi.com/2032-6653/11/4/77

[21] G. Gunlu, "Dynamically Reconfigurable Independent Cellular Switching Circuits for Managing Battery Modules," *IEEE Transactions on Energy Conversion*, vol. 32, no. 1, pp. 194–201, 3 2017.

[22] V. Viswanathan, L. N. Palaniswamy, and P. B. Leelavinodhan, "Optimization techniques of battery packs using re-configurability: A review," *Journal of Energy Storage*, vol. 23, pp. 404–415, 6 2019.

[23] S. E. O'Kane, W. Ai, G. Madabattula, D. Alonso-Alvarez, R. Timms, V. Sulzer, J. S. Edge, B. Wu, G. J. Offer, and M. Marinescu, "Lithium-ion battery degradation: how to model it," *Physical Chemistry Chemical Physics*, vol. 24, no. 13, pp. 7909–7922, 2022.

[24] C.-H. Chen, F. Brosa Planella, K. O'Regan, D. Gastol, W. D. Widanage, and E. Kendrick, "Development of Experimental Techniques for Parameterization of Multi-scale Lithium-ion Battery Models," *Journal of The Electrochemical Society*, vol. 167, no. 8, p. 080534, 1 2020.

[25] W. Vermeer, G. R. Chandra Mouli, and P. Bauer, "A Comprehensive Review on the Characteristics and Modeling of Lithium-Ion Battery Aging," *IEEE Transactions on Transportation Electrification*, vol. 8, no. 2, pp. 2205–2232, 6 2022.